An Innovative Lens Type FinLine to Microstrip Transition

L. Valletti[1] · S. Fantauzzi[1] · F. Di Paolo[1]

Abstract

Due to the disadvantages of vacuum tubes in terms of warm-up time, size, and high-voltage needs, solid-state power amplifiers (SSPAs) with gallium nitride (GaN) monolithic microwave integrated circuits (MMICs) are the key solution for power levels up to some kilowatts in continuous wave. An SSPA is the most convenient solution for these RF power levels due to its low weight, small size, negligible warm-up time, low-voltage operation, and high reliability. Spatial power amplifiers (SPAs) combining techniques are the best candidates for SSPAs due to the intrinsic low attenuation in dividing and combining functions. SPAs mainly use two types of probes: transverse and longitudinal, such as FinLines. This paper describes a broadband FinLine to microstrip (FLuS) transition based on dielectric lens theory. Comparative simulations with traditional FinLine transitions show a significant improvement in matching performances and a very significant increase in mechanical resistance of the transition. The proposed innovative FLuS uses a substrate shaping designed according to dielectric lens theory. Frequency simulations of a FLuS inside the WR22 waveguide are shown. These evidence the better performances of this transition than the classic FLuS transition using quarter-wave transformer (QWT) matching. A Q band spatial power combiner with dielectric lens FLuS was made and measured, showing the excellent performances of this innovative FLuS transition.

Keywords FinLine to microstrip transitions · Q band · Dielectric lens · Spatial power combiners · Multiphysics simulations

1 Introduction

Spatial power amplifiers (SPAs) [1] are the most desired components whenever small size, solid-state high-power density, and graceful degradation are needed; like in strategic electronic warfare (EW) and electronic counter measurement/electronic

✉ L. Valletti
  lorenzo.valletti@uniroma2.it

1 Department of Electronic Engineering, University of Roma Tor Vergata, Rome, Italy

⚛ Springer

counter counter measurements (ECM/ECCM) systems, and space communications applications. To avoid confusion between the field of power amplifiers (PAs) for space applications and the effective way of combining amplifiers, SPAs should be named wave front amplifiers (WFAs). However, the SPA name is now established, and this will be used in the following of this paper.

With the available RF output power of solid-state devices, an SPA is confined to output power levels less than some kilowatt at X band, even less for higher operating frequencies. However, considering the output power as the only important aspect of power amplifiers, the vacuum tube technology has the leadership since extremely high RF powers can be reached, especially for pulsed applications [2, 3].

FLuS can be regarded in our case as Vivaldi [4] inside the waveguide. Vivaldi antennas are widely used in broadband applications. Recently, such antennas have also been studied working at THz frequencies [5], a frequency range very useful for energy micro unmanned air vehicle (UAV) harvesting applications [6–8].

Recent advances in GaN technology allow us to obtain solid-state high-power amplifiers (SSHPAs) at high frequencies and with high reliability. The GaN efficiency performed better than the consolidated GaAs technology [9]. However, many devices need to be combined to get a system with higher RF power capability than a single device. Several combining techniques exist [1], and recent advances in using transverse probes seem attractive [10] for RF power applications. However, combining techniques using longitudinal probes, like FinLines, have been widely proven to be very useful for SPAs in terms of operating bandwidth [1, 11–19] in compactness and, consequently, high power density. Longitudinal probes also have practical applications in mode converters [20], mixers [21] as well as in other applications [22]. The proposed innovative FinLine to microstrip (FLuS) transition uses a substrate shaping designed according to dielectric lens theory; an application of this transition in SPA technology is reported. Frequency simulations are shown for FLuS inside a WR22 waveguide, which evidences the better performance of this transition than the classic FLuS transition using quarter wavelength matching.

This paper is organized as follows. In "Section 2," a brief introduction of the FLuS implementation in spatial power combining is given. In "Section 3," the design procedure of the innovative FLuS is reported.

Simulations and results of the proposed transition are given in "Section 4." "Section 5" shows measurements made on a passive Q band spatial power combiner using a WR22 waveguide FLuS with the dielectric lens. Finally, in "Section 6," the conclusions of this work are given.

2 Longitudinal Probe SPA Fundamentals

The SPA is an amplifier where N active devices are arranged in a propagating media, thus:

- an EM field feeds each active device with an amplitude of $1/N$ of the EM field at the amplifier's input.

- the division/combining operation by N is possibly realized by M steps, as low as possible.

This general concept is shown in Fig. 1.

So, the ideal SPA would have $M = 1$ step of divisions and $N = \infty$ number of amplifiers, but some compromises are practically necessary. A fundamental block of SPAs is the spatial power combiner (SPC), which is a passive reciprocal device that, for this reason, can also be called spatial power divider (SPD). The SPC (or SPD) performs a parallel combining (or dividing) operation of many RF signals, thus reducing the combining (or dividing) loss to a minimum value. In SPC, electromagnetic probes are used; these capture the incoming signal and send the amplified signal inside the medium, usually air. Depending on the type of SPA [9], the most used probes are longitudinal, like FinLines, or transversal [1, 10]. Such probes are necessary to transform input electrical field polarization to required MMIC electrical field polarization, usually a qTEM mode.
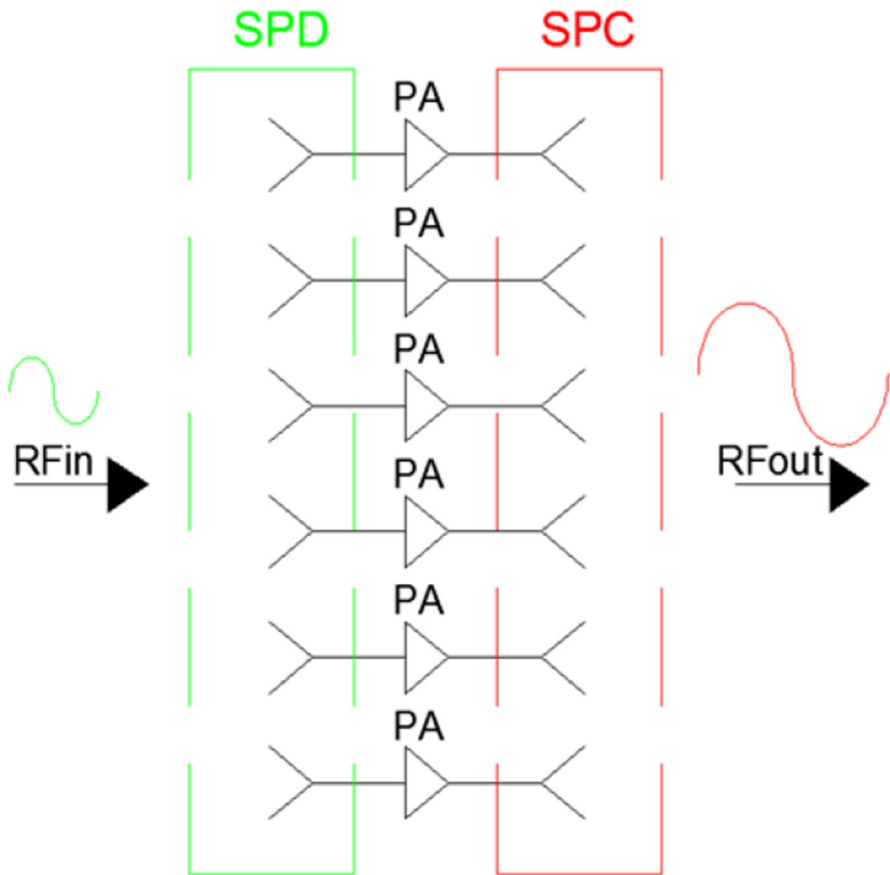

Fig. 1 The general spatial power amplifier concept

This parallel combining/dividing characteristic of SPAs is utterly different from any other classical approach to combining power signals. For instance, the classical binary technique consists of a tree structure where the signals are added by binary combiners such as Wilkinson power combiners [23].

This solution is limited by the losses each combiner inserts; this architecture also limits the number of devices used, which can only be a power of two. Conversely, spatial power combiners are based on signal power combination with low loss propagation inside the space of a transmission line or even in open space [1]. When the signal combining and dividing are realized in a closed space, several advantages occur, such as high device compactness, low combining loss, and, consequently, high RF output power. SPA can, in many cases, replace power vacuum tubes, providing a low-weight structure that works at low voltages with high reliability and great graceful degradation [14].

The basic concept in SPAs is to combine as many active devices as possible, in the most negligible possible volume and with the smallest possible weight. Many considerations have to be made for the design, such as active device supply routing, possible unwanted oscillations analysis, and effective heat management. The SPA family is composed of different types. They differ from each other by the propagating modes in the medium. Examples are TEM and non-TEM spatial combiners, cavity-based, open space ones. Detailed information regarding such types has been given in [9].

A classic non-TEM SPA comprises three parts: waveguide, probes, and a qTEM cavity where MMIC PAs are placed. In Fig. 2, we show an example of a SPA using longitudinal probes, a FinLine to double microstrip (dual FLuS) transition [24].

An exponential profile for the antipodal dual FLuS conductors has been chosen [14] according to (1).

$$w(z) = w_0 \left\{ e^{\frac{z \, \ln(w_f)}{L_{Fin}}} - 1 \right\} \tag{1}$$

w_f is the parameter that determines the curvature of the FLuS. It must be $0 < w_f < 1$, and for $w_f \to 1$, the exponential verges to a line; this is the parameter that weights more on the transformation, and it has the same behavior as the ratio of the turns in a coil transformer. L_{Fin} is a free parameter; it determines the longitudinal length of the transition. The geometric boundary conditions are (2) and (3).

$$w(0) = 0 \tag{2}$$

$$w\left(z = L_{Fin}\right) = -\frac{w_{50} + w_{sub}}{2} \tag{3}$$

where w_{sub} is the width of the substrate: the FLuS fits on the E plane, so this value coincides with the short side of the guide; w_{50} is the width of the output microstrips to have 50 Ω of transmission line impedance [25]. The parameter w_0 is obtained from the boundary conditions and shown in (4).
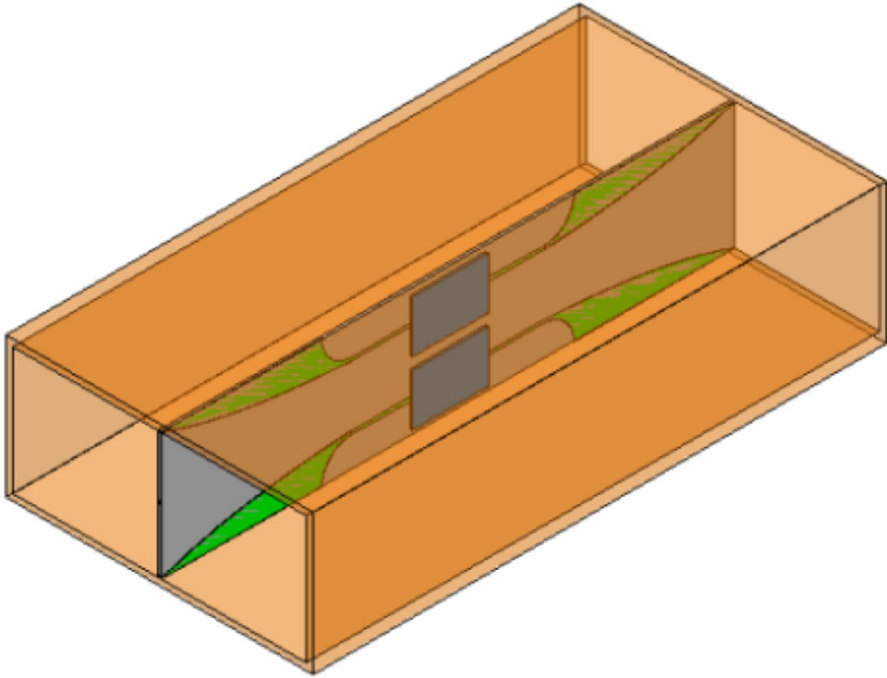
Fig. 2 Basic model of SPA inside rectangular waveguide

$$w_0 = \frac{w_{50} + w_{sub}}{2 \cdot (1 - w_f)} \qquad (4)$$

The tapered profile matches the impedances of the TEM mode of the microstrip and the TE_{10} mode of the waveguide. The equation shown in (1) is applicable for the design of FinLine with multiple microstrips port with some modifications [22, 26].

The sharp transition between the vacuum and the probe substrate creates a considerable discontinuity that worsens the matching of the amplifier. Therefore, carrying out an impedance transformation through the substrate is also necessary. A simple way is to insert a quarter-wave transformer (QWT) just before the Fin, i.e., an additional substrate segment, a quarter of wavelength long. A double FLuS and QWTs are shown in Fig. 3.

A quarter-wave transformer cannot have broadband behavior due to the abrupt dielectric discontinuity passing from air or vacuum inside the waveguide to the FLuS substrate. In addition, the sharp corners of the quarter-wave segment still have discontinuities. A simple solution is to make more transformation steps at $\lambda/4$, gradually reducing the width of each added step, as shown later. It is an effective solution but limited by the intrinsic fragility of the substrate, which becomes even more critical when FLuS are used in small waveguides. Other matching techniques [27] have shown significant performance but could compromise the mechanical integrity of the transition.
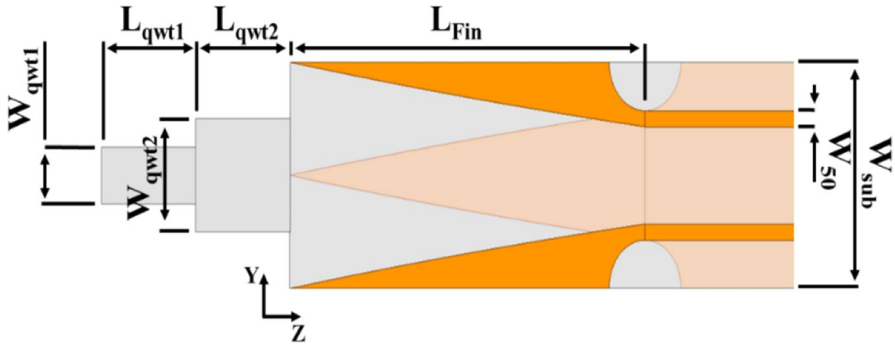
Fig. 3 Dual FLuS geometry

From a purely electromagnetic point of view, it is necessary to focus most of the field inside the FLuS in the transition direction. In optical devices, this type of behavior is known as lenses. The following section discusses applying such a concept to a FLuS.

3 Novel FinLine Lens Design Procedure

The "dielectric lenses" in microwaves are studied with geometric ray optics. Snell's law in (5) is considered:

$$\frac{\sin \theta}{\sin \theta'} = \frac{n_2}{n_1} = n_{21} \tag{5}$$

where θ and θ' are the inclination angles of incident and refracted rays in the lens with respect to the perpendicular direction to the interface. $n = \sqrt{\epsilon_r \mu_r}$ is the refractive index. The geometry of Snell's law is reported in Fig. 4.

It has been demonstrated [28] that the vector of a wave incident on an interface can be divided into two components, E_{0y} and E_{0v}; therefore, we have $E = E_{0y}y_0 + E_{0v}v_0$. In Fig. 4, the medium "1" is considered the vacuum of the waveguide, while the medium "2" is alumina, the material of the FLuS substrate. Considering $\epsilon_r^a = 9.8$, we have $n_2 = \sqrt{9.8} \approx 3.13$.

The voltage reflection R_s and voltage transmission T_s coefficients of the E_{0y} component are defined in (6) and (7).

$$R_s = \frac{E_{0y}''}{E_{0y}} = \frac{n_2 \cos \theta - n_1 \cos \theta'}{n_2 \cos \theta + n_1 \cos \theta'} \cong \frac{\cos \theta - \sqrt{\epsilon_r^a - \sin^2 \theta}}{\cos \theta + \sqrt{\epsilon_r^a - \sin^2 \theta}} \tag{6}$$
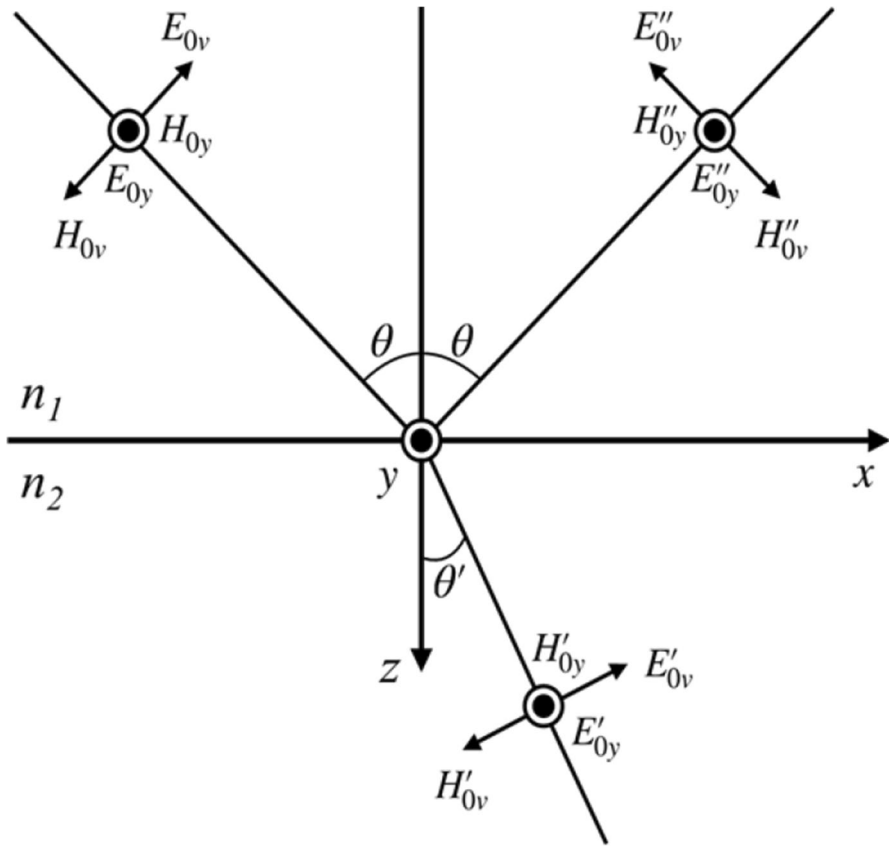
$$T_s = 1 - R_s \tag{7}$$

Fig. 4 Components of the electric and magnetic vectors at the interface between two different dielectrics

If n_2 increases because of the increase of ϵ_r, the modulus of the reflected wave increases; therefore, the modulus of the refracted wave decreases; this electromagnetically explains the mismatch introduced by alumina. Moreover, for the law of Snell, the angle θ' reduces. The E_y component of the TE10 mode of the guide always has a linear polarization perpendicular to the direction of propagation, and the wavefronts are parallel planes.

Considering an ellipsoidal dielectric lens, such as the one in Fig. 5, it has been demonstrated [29] that this geometry transforms a spherical wave into a planar wave and vice versa by applying Snell's law on infinitesimal sections of the curved profile.

The eccentricity e of the ellipse is linked to the permittivity of the substrate as follows in (8):

$$e = \frac{f}{a} = \epsilon_r^{-\frac{1}{2}} \tag{8}$$

with f the focal length given by (9)
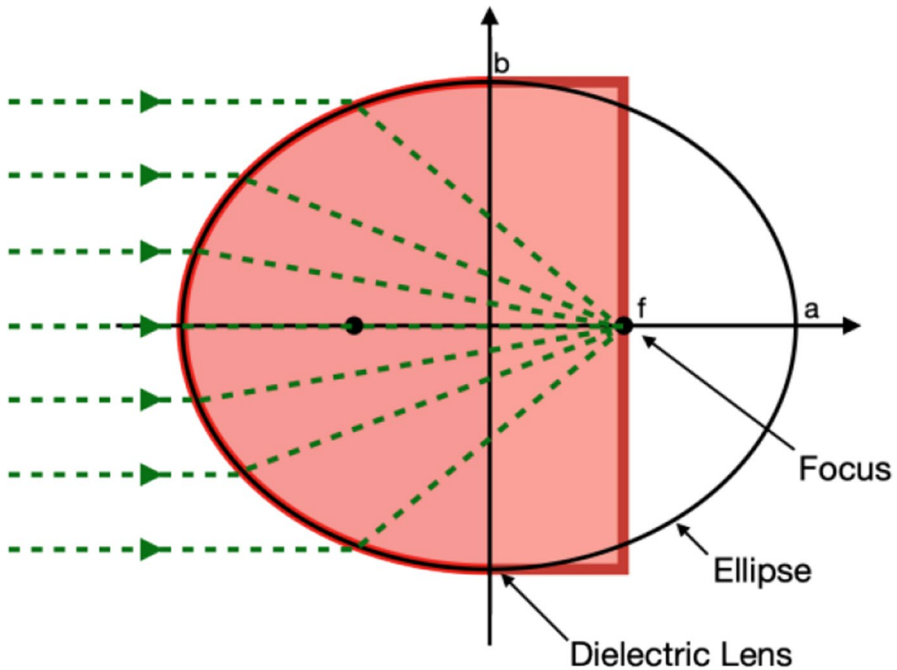
Fig. 5 Ellipsoidal dielectric lens

$$f = b(\epsilon_r - 1)^{-1/2} \tag{9}$$

where *b* is the length of the minor axis. The higher the dielectric permittivity value, the lower the ratio between the ellipse axes, as shown in Fig. 6.

The same type of conductor profiles, described in "Section 2," has been used for both standard FLuSes and the new lens type FLuS proposed in this work. Consequently, individual profiles have been optimized for each FLuS through HFSS simulations.

4 Simulation Results

In the first part of this section, we discuss the frequency domain simulations for the various FLuSes. Then in "Section 4.2," we report the stress–strain simulations of the dual QWT and the lens type FLuSes. The substrate used for these FLuSes is alumina 99.8% with a thickness of 254 μm, while conductor traces are realized in gold with a thickness of 4 μm.

4.1 Frequency Domain Simulations

Various types of FLuS have been compared, including the simplest FLuS with no QWT matching. Each FLuS is inserted inside a WR22 waveguide, as shown
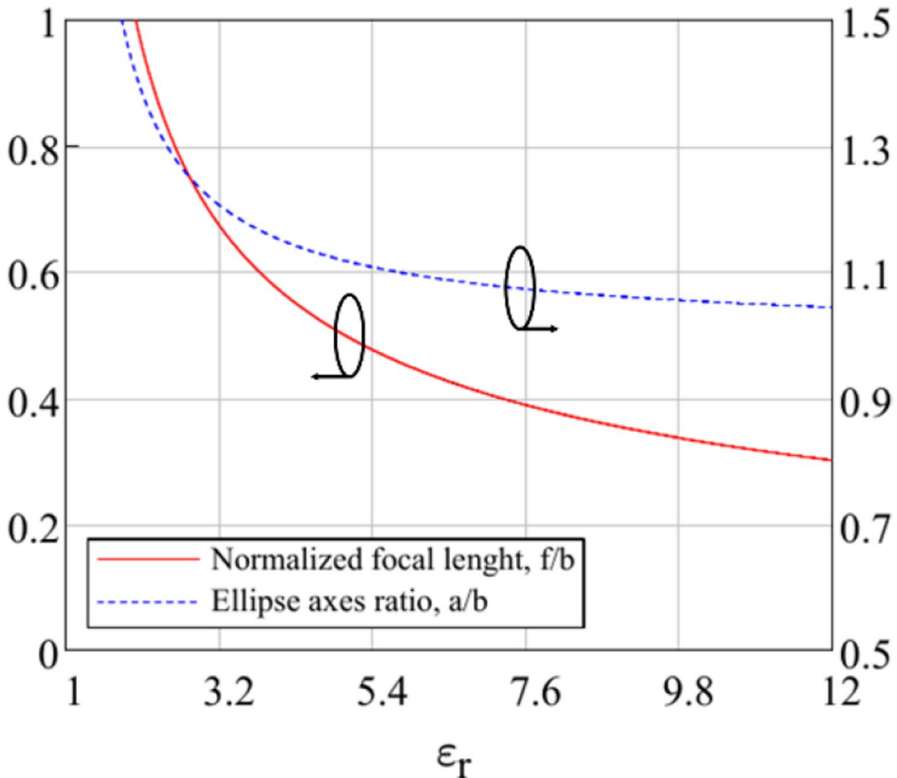
Fig. 6 Ellipse axis ratio and normalized focal length vs. permittivity

in Fig. 7, so three ports can be defined: one waveguide port and two microstrips ports. The length of the microstrip lines at the end of the FLuS is 2.5 mm, while the total length of the simulated structure, i.e., the WR22 waveguide, is 20 mm. Each FLuS structure is independently optimized for the best 33–50 GHz band results.

The significant electromagnetic values are return loss (RL) of waveguide port, RL of one microstrip port, and insertion loss (IL) between these two ports, respectively S11, S22, and S21 in terms of scattering parameters, S33 and S31 are identical to S22 and S21, because of symmetricity of the network. The best performances for the simple dual FLuS without QWT are reported in Figs. 11, 12, and 13. A mean IL of nearly 3.35 dB is obtained, with an RL on the waveguide port (RL_{WG}) of at least 15 dB. After subtracting 3 dB of power division from the results, we notice that the structure loses nearly 0.35 dB.

The matching on the microstrip port ($RL_{\mu s}$) is consistent with the theory of lossless three-port networks [25, 28]; in fact, an ideal 3-port transformer can only reach a minimum RL of 6 dB on the splitting signal ports. This phenomenon is well known in the design of SPAs; further stages of Wilkinson dividers are usually added to the microstrip network to improve matching and avoid loops [1].
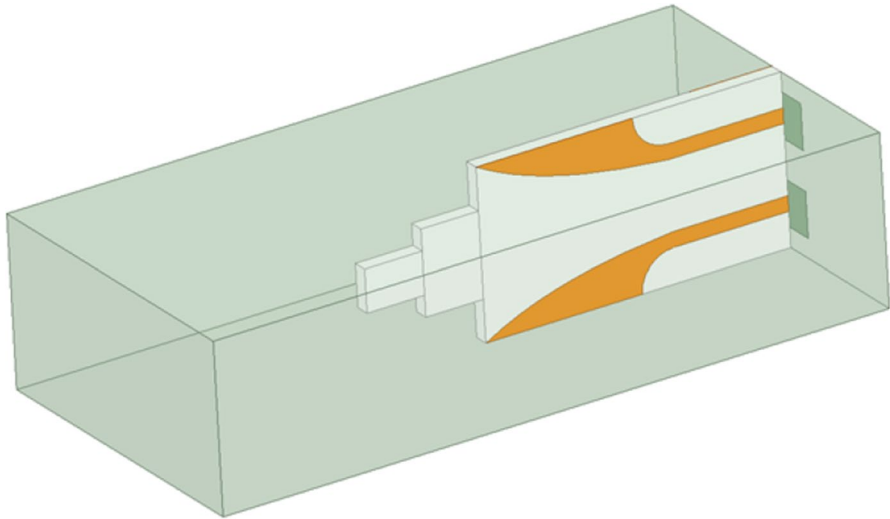
Fig. 7 FLuS inside WR22 waveguide with QWT, ready for simulation

The second structure we compare introduces a FLuS with two QWT matching sections, as shown in Fig. 3. The width of any QWT section halves in respect of the width of the previous one. However, dual QWT is critical for small waveguides since the first QWT becomes very narrow, and the fragility of the structure cannot be accepted for applications where vibrations are concerned. This dual QWT FLuS design guarantees better matching on the waveguide port, as shown in Figs. 11, 12, and 13, with a similar IL and far better RL.

Table 1 shows the dimensions of the two QWT steps; it is possible to notice that the first QWT has a very thin width, which is critical from a mechanical point of view, as will be analyzed later in this document.

The third design is shown in Fig. 8 and consists of a FLuS with an ellipsoidal dielectric lens (EDL) matching section. As shown later, this shape is more mechanically sturdy than the dual QWT shape.

The simulated performances are shown in Figs. 11, 12, and 13. We recognize that waveguide port matching is better than the QWT case but with the same IL. A mean IL of 3.35 dB is obtained, with a RL on the waveguide port greater than 15 dB for the entire Q band and greater than 20 dB for 34–50 GHz. After subtracting 3 dB of power division, the structure introduces a loss of nearly 0.35 dB.

Figure 9 shows the parametric variation of the ellipse axes ratio, considering the minor axis fixed.

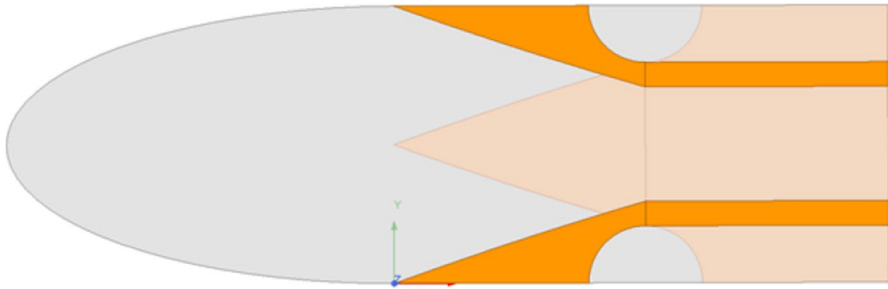| Table 1 Q band QWT dimensions	QWT	Length (mm)	Width (mm)
	1	1.2	0.71
	2	1.1	1.39

Fig. 8 FLuS with EDL matching

For an ellipse axes ratio of 2.8, there is the optimum of the mean RL on the waveguide. Therefore, considering a semi-axis fixed to the half-value of the short side of the WR22, that is, 1.4224 mm, we have $f = 2.56$ mm. From Eq. (9), we obtain an ϵ_r value of 1.31. The substrate matching, which has $\epsilon_r = 9.8$, occupies about 4% of the volume, and the rest is vacuum; therefore, the weighted average of the ϵ_r value of the substrate transition is $\epsilon_{r,avg} = 0.96 \cdot 1 + 0.04 \cdot 9.8 = 1.35$, considering any non-idealities of the structure, the calculated value is consistent with the value obtained in the simulation.

The last structure we analyze is the FLuS with parabolic dielectric lens (PDL), as shown in Fig. 10. This shape has a length comparable to the EDL.
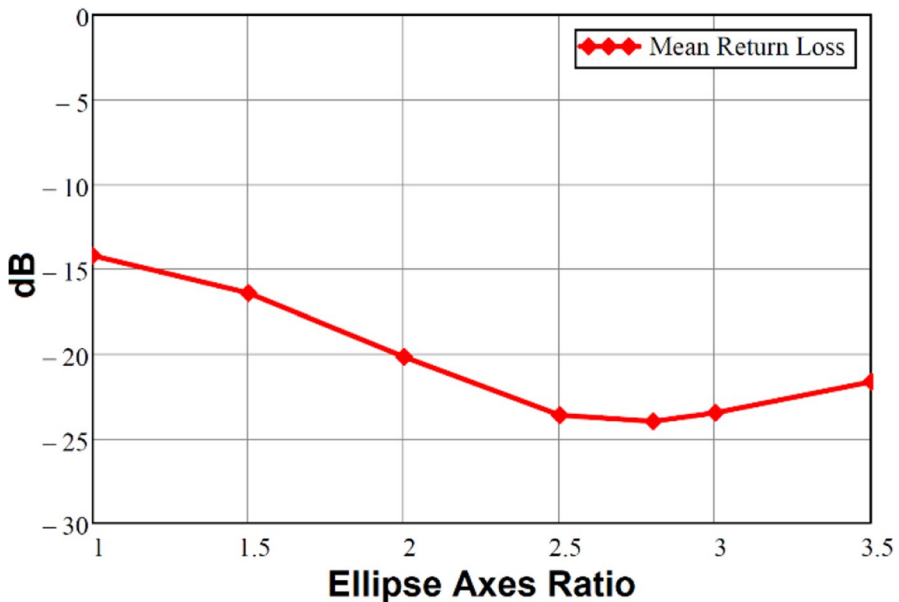
Fig. 9 Mean return loss as a function of ellipse axes ratio
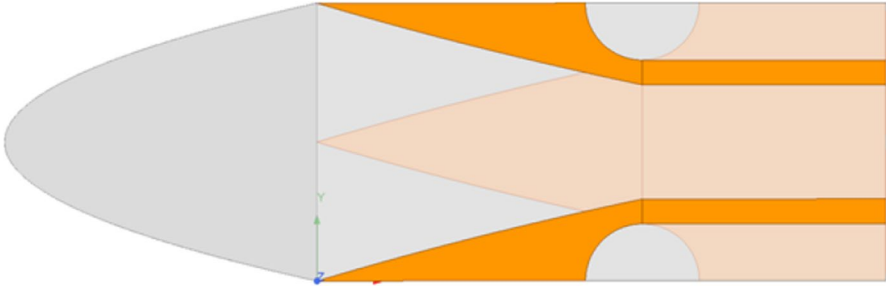
Fig. 10 FLuS with PDL matching
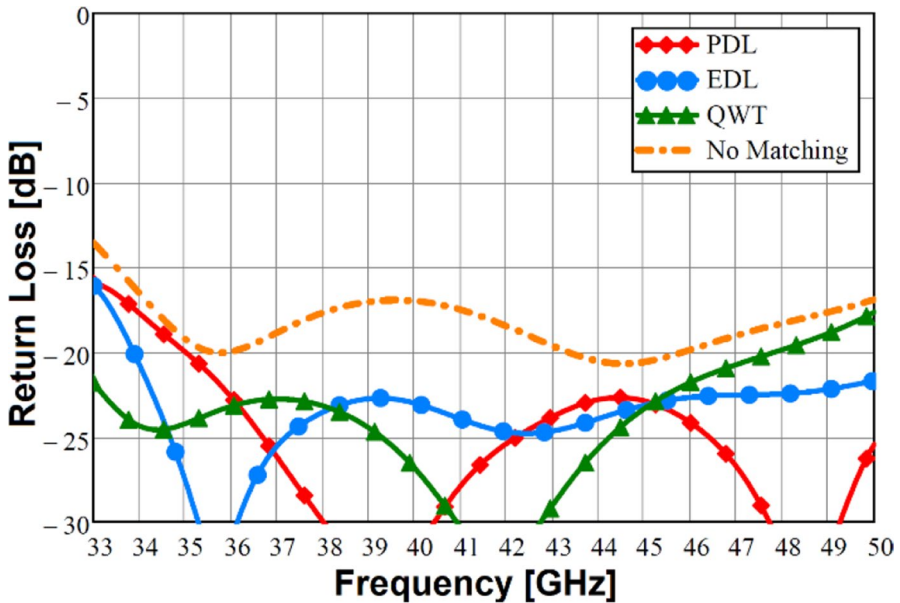
Fig. 11 Return loss of the optimized FLuSes

Performances are reported in Figs. 11, 12, and 13. A mean IL of 3.4 dB is obtained, with a RL on the waveguide port greater than 15 dB for the entire Q band and greater than 20 dB for 35–50 GHz. The structure introduces a loss of nearly 0.4 dB. We recognize that the RL at the waveguide port is good in any shown substrate matching: in any case, performances are better than FLuSes without any matching.

The microstrip port matching does not substantially vary between the simulated designs.
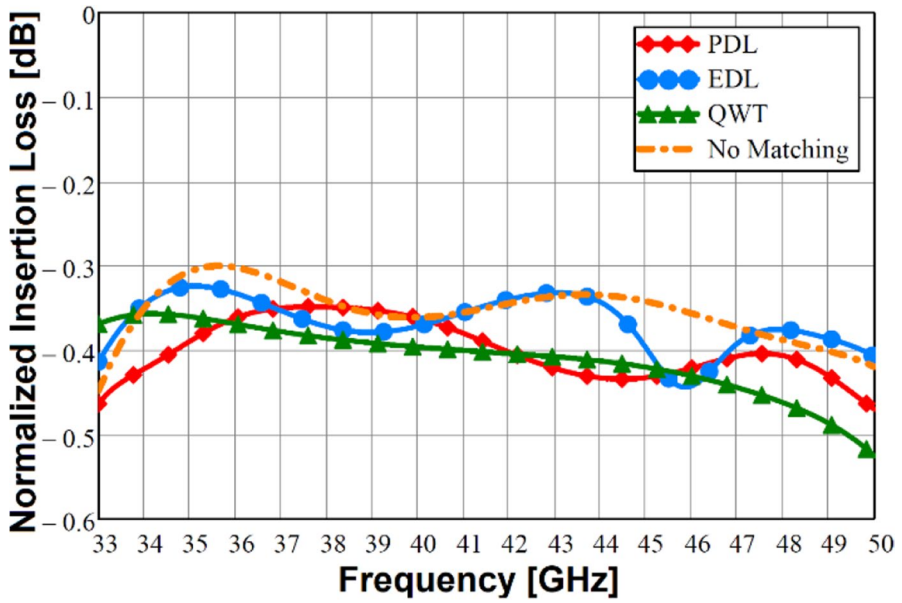
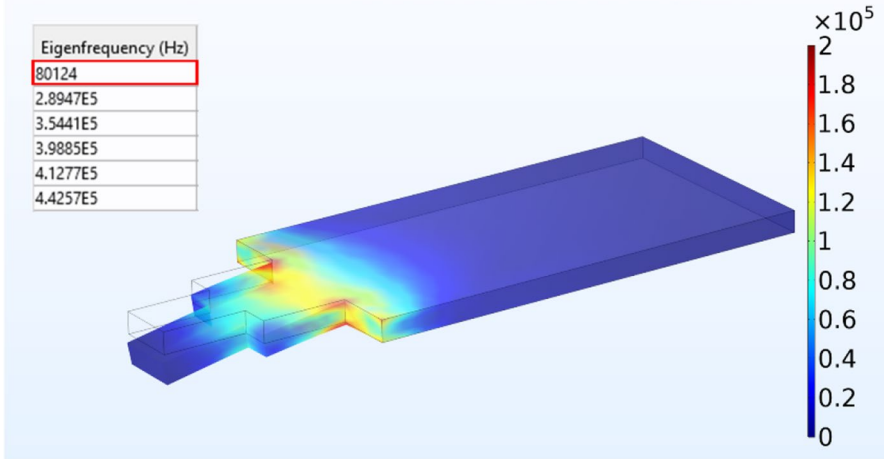**Fig. 12** 3 dB normalized insertion loss of the optimized FLuSes
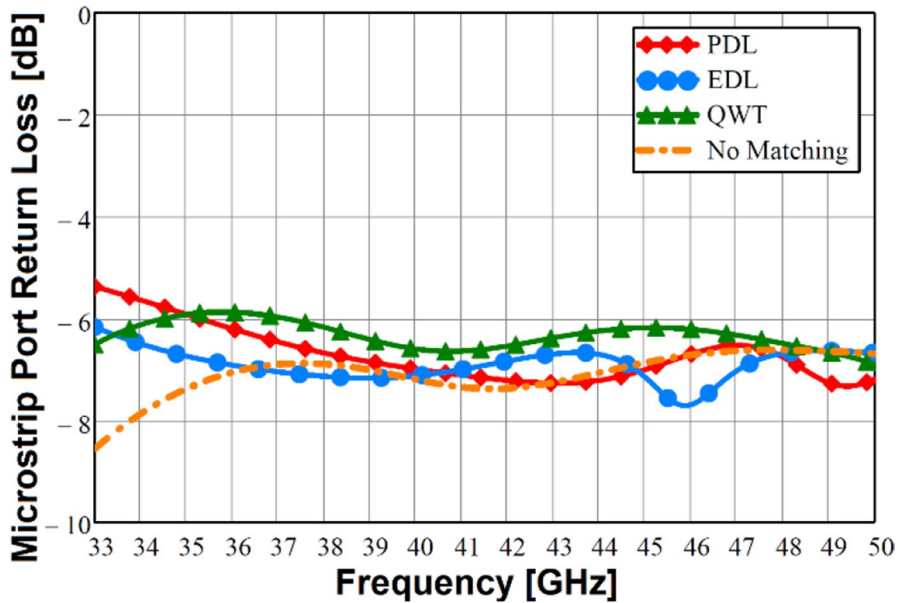
Fig. 13 Microstrip port return loss of the optimized FLuSes

Table 2 FLuSes critical dimensions and parameters

Type	L_{Fin} (mm)	Substrate matching length (mm)	w_f
QWT	3.3	2.3	0.15
PDL	3.3	3.2	0.7
EDL	2.6	4	0.8

Fig. 14 3D distribution of Von Mises stress in FLuS with QWT and the obtained eigenfrequencies

4.2 Structural Mechanics Simulations of the Dielectric

In practice, any electronic system subjects vibrations. A satellite module, for instance, experiences different types of vibrations reproduced during several preliminary tests. Vibrations that occur in the sinusoidal regime and random vibrations are the most tested, but also a pyrotechnic shock is applied to the entire space module. The maximum mechanical resonant frequency tested stands at 10 kHz. Each part of the system which presents fundamental mechanical resonance frequencies above the value of 10 kHz [30] is structurally qualified for space applications. Stress and strain analysis is necessary and should be done in any practical electronic system; in particular, vacuum applications require investigation of possible defects during operative conditions [31, 32]. For this reason, we have investigated the stress and the strain of the FLuS with dual QWT and PDL using COMSOL software version IV.

For comparison purposes, considering Figs. 3, 8, 10, and Eq. (4), in Table 2 are reported the design values of the presented FLuSes.

In Fig. 14, we report the stress and the first six eigenfrequencies for the case of the dual QWT FLuS.
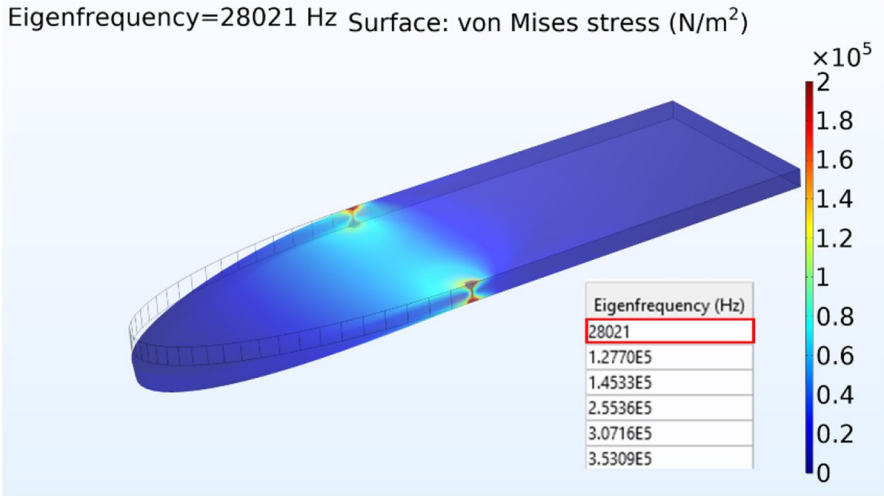
Fig. 15 3D distribution of Von Mises stress in FLuS with EDL and the obtained eigenfrequencies
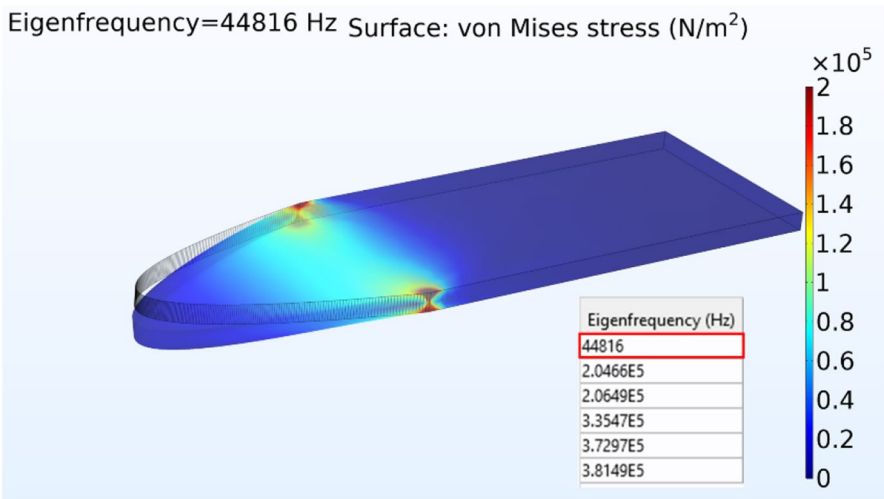

Fig. 16 3D distribution of Von Mises stress in FLuS with PDL and the obtained eigenfrequencies

Then we analyzed the FLuS with EDL and PDL, obtaining stress and the first six eigenfrequencies as shown in Figs. 15 and 16.

For a better comparison between the FLuSes versions, an integration line along the z-direction (considering Fig. 3) has been considered at the top face of both FLuS. The stress and the displacement at first eigenfrequency (outlined in red) have been analyzed over the defined integration line; Figs. 17 and 18 show the results.
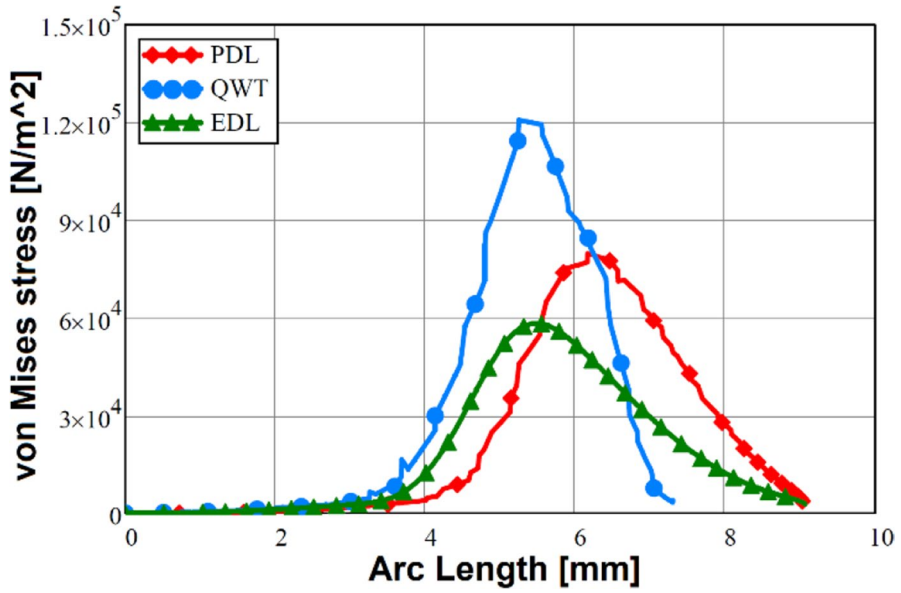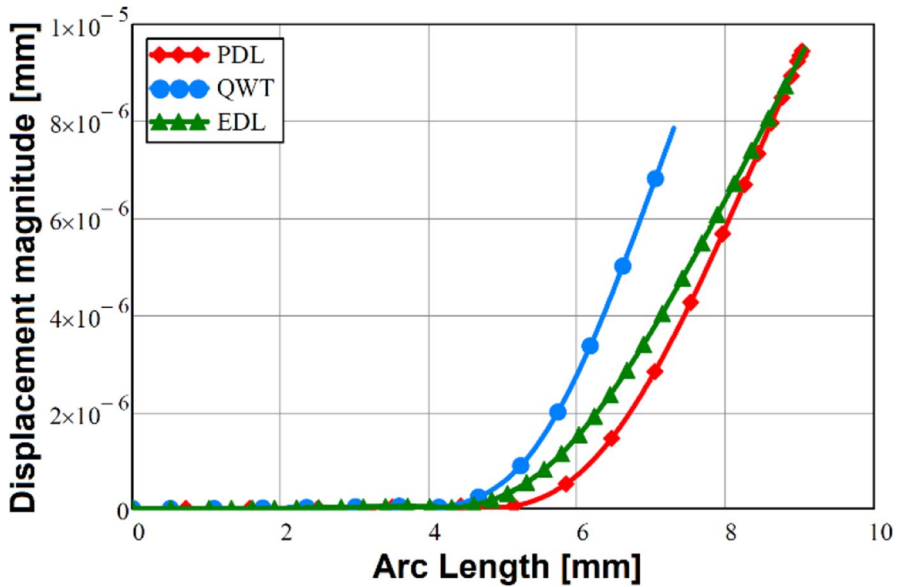
Fig. 17 Von Mises stress in the FLuSes

Fig. 18 Displacement of the FLuSes

Table 3 Summarized simulation results

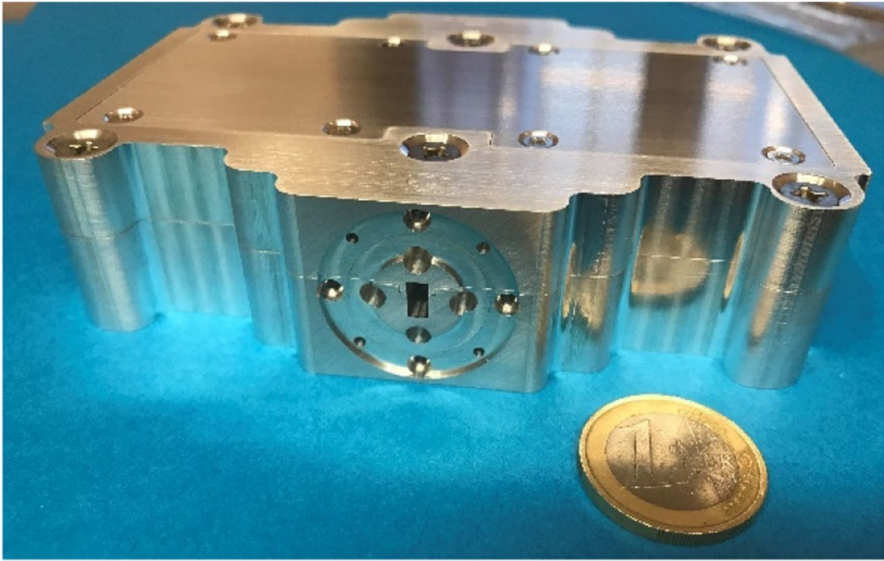| Type	RL_{wg} min (dB)	$RL_{\mu s}$ min (dB)	IL^1 min (dB)	RL_{wg} max (dB)	$RL_{\mu s}$ max (dB)	IL^1 max (dB)	First E.F. (KHz)	V.M. stress max (N/m^2)
QWT	17.6	5.9	3.4	32.2	6.9	3.5	80.12	1.2×10^5
PDL	16	5.4	3.3	33	7.3	3.5	44.82	0.8×10^5
EDL	16.1	6.2	3.3	32.3	7.7	3.4	28.02	0.58×10^5

[1]Considering 3 dB of power division

Fig. 19 Measured Q band spatial power combiner prototype

From the above results, we can recognize how smaller stress occurs in the FLuS with PDL and EDL in respect of the one with dual QWT. Furthermore, the first eigenfrequency highly depends on the substrate matching length.

In Table 3, we summarize the results for the FLuS analyzed in detail in this work.

Based on these results, we recognize the better mechanical performances of FLuSes with the dielectric lens than the classical QWT FLuS.

5 Measurements

The university of Rome "Tor Vergata" designed a Q band spatial power combiner [33]. Following the procedure reported above, a double FLuS was designed for the WR22 waveguide. MITEC-Roma manufactured the prototype shown in Fig. 19. The SPA that can be realized starting from the passive structure proposed in [33] operates in the Q band, and it combines the power of 16 MMICs, eight of which are placed on the top side and the other eight on the bottom side. For the realization of the proposed prototype, a non-TEM SPC architecture was chosen and realized in the WR22 waveguide; the block diagram is shown in Fig. 20.

The input power injected from the external waveguide port in the SPC is firstly divided by an E-plane waveguide T-junction. Then power is divided by two back-to-back double FLuS into four microstrip lines for each T-junction branch.

A set of Wilkinson dividers placed right before the solid-state power amplifiers makes a final step of power division. Wilkinson dividers split the power into 16 microstrip branches. The power is recombined with a specular passive network.
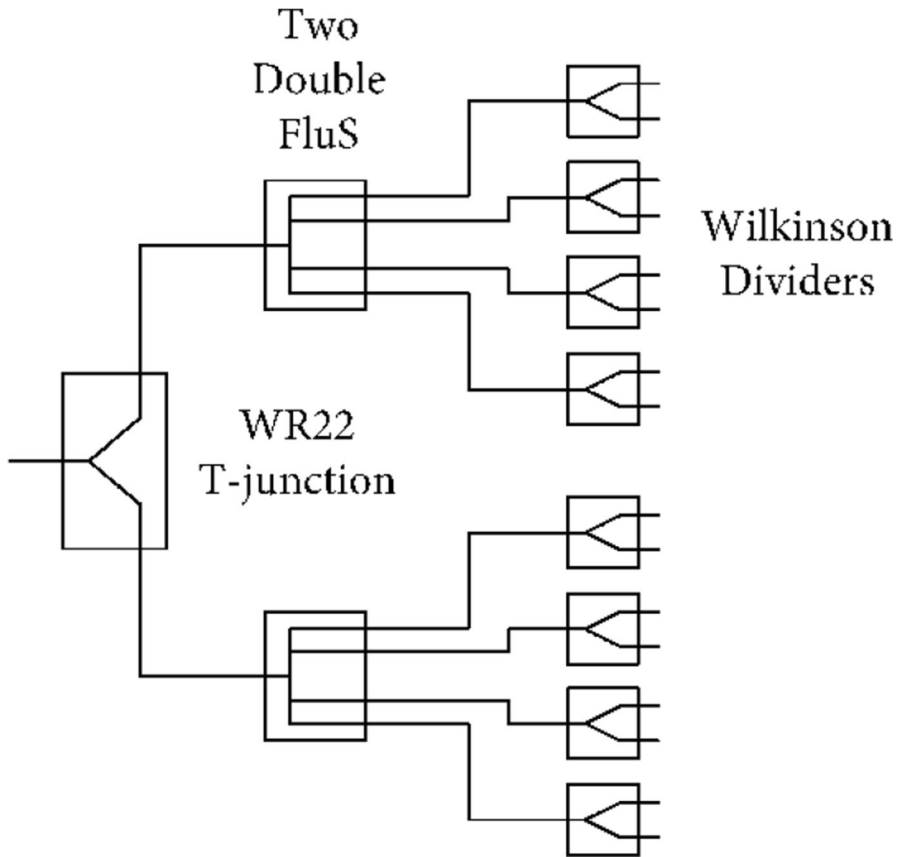
Fig. 20 Block diagram of half SPC

Due to the critical dimensions of QWT in stepped FLuS, the design was oriented to use the parabolic dielectric lens FLuS shown in Fig. 10.

As described in "Section 4.1," the PDL FLuS structure was synthesized and optimized across the whole Q band (33–50 GHz). FLuS performances are reported in Figs. 11, 12, and 13. To get a clearer picture of the FLuS behavior with PDL matching, a configuration of two back-to-back FLuSes with 6 mm length microstrips was simulated. The results are shown in Fig. 21.

The length of the microstrip of the FLuS was reduced to the minimum possible to minimize losses. Moreover, for the same reason, Rogers Duroid 5880 substrate was used in microstrips. Since, for the same characteristic impedance, Duroid microstrips are wider, it was necessary to use alumina as a substrate in FLuS and in Wilkinson dividers. The entire SPC simulated is shown in Fig. 22, and the S-parameters obtained are shown in Figs. 25 and 26. Realized FLuS is shown in Fig. 23.
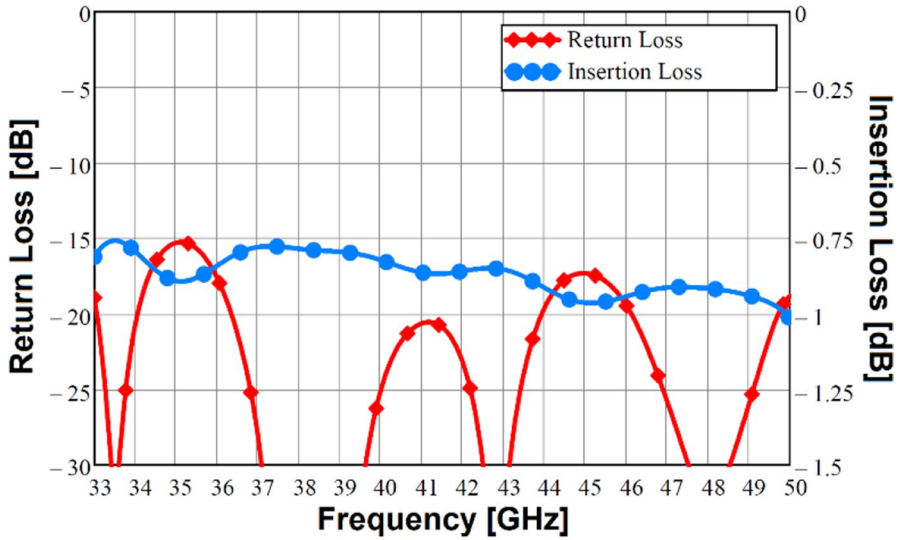
Fig. 21 S-parameters of a back-to-back configuration of two Q band FLuSes
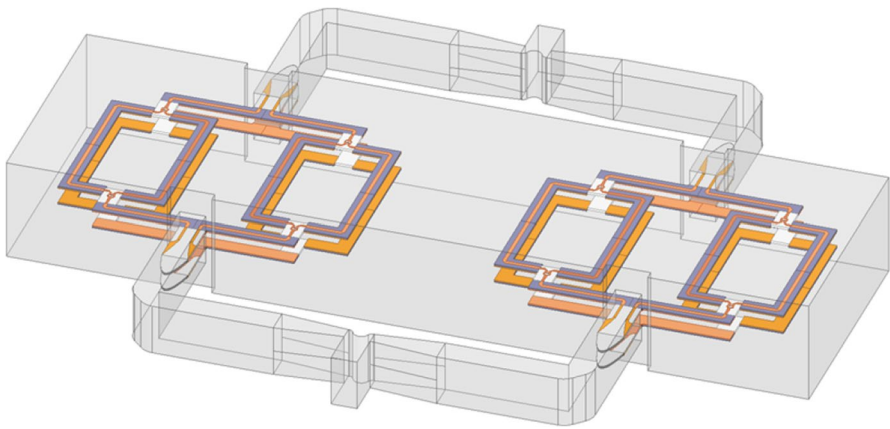

Fig. 22 Simulated full SPC with WR22 ports

The test bench used for the prototype measurements consists of a vector analyzer, two coaxial cables, and two coaxial to WR22 waveguide transitions, as shown in Fig. 24. The vector analyzer is a Rohde & Schwarz ZVA50 with capabilities up to 50 GHz. On the other hand, the calibration kit available for measurements was for the Ka band (up to 40 GHz) due to a limited budget. Measurements were performed in SDS Laboratories in Rome.

Since the structure is passive, the only significant electromagnetic values to measure are the S11 (RL) and S21 (IL). The other two scattering parameters, S22
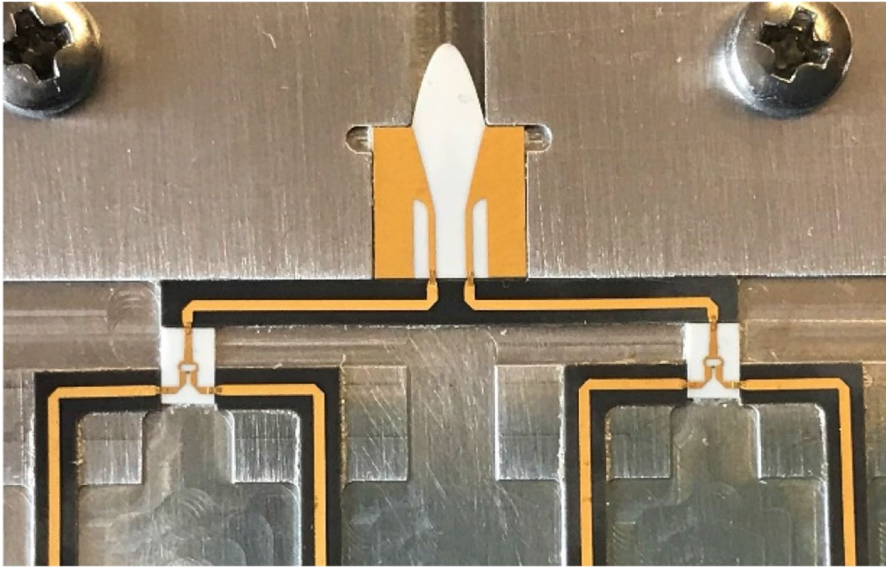
Fig. 23 Upside FLuS and Wilkinson dividers bonded to Duroid substrate microstrips

and S12, are identical to the previous ones because of the reciprocity property of a passive network [25]. These measures were carried out over the entire bandwidth covered by the WR22 waveguide, from 33 to 50 GHz, i.e., the entire Q band.

Figures 25 and 26 show the broadband behavior of the measured SPC, a value below 10 dB in terms of RL over the whole bandwidth of the waveguide.

Regarding the IL, bandwidth is narrower, and it is possible to consider this structure exploitable up to a frequency of 47 GHz. After 47 GHz, there are visible resonances on IL; the use of a cal-kit limited to the Ka band could justify this behavior. The mean value of IL shown up to this frequency is about 4 dB, but it is essential to consider that this is the value of the losses between the input and output ports. In the final spatial power amplifier, the critical value in terms of efficiency is the IL of the path starting from the output pad of the MMICs and ending at the output waveguide port. The solid-state power amplifiers are usually placed in the center of the SPC since the structure is symmetrical. So, it is reasonable to estimate that the output losses of the Q band amplifier will be practically the half value of the losses of the entire passive SPC, then 2 dB. With such a value of S21, the Q band spatial power amplifier will present a combining efficiency of 65%.

Table 4 compares the performance of the transition reported in this work and the performance of the FLuS and other waveguides to microstrip transitions. Structures operating in the Q and Ka bands are considered, showing 10 dB RL fractional bandwidths.
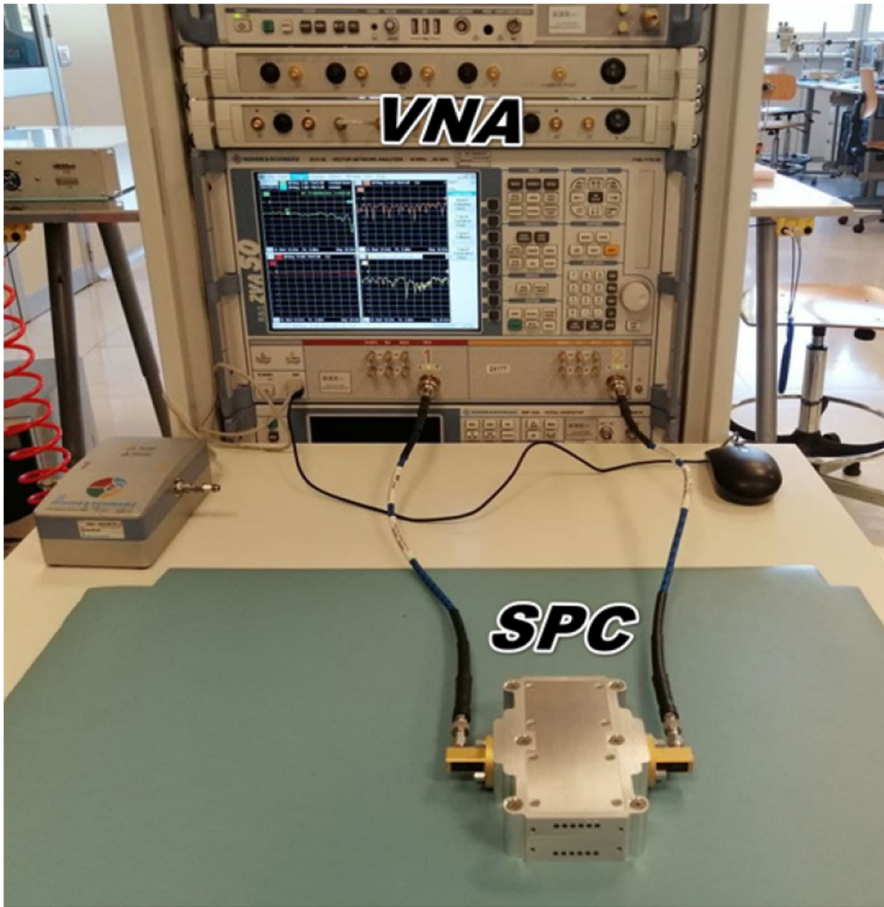
Fig. 24 Q band SPC test bench

With 65% of efficiency, using commercial MMICs, each with 10 W of output power, the RF output power of the spatial amplifier will be over 100 W in the Q band spectrum.

6 Conclusion

In this work, novel FinLine to microstrip transitions have been studied. They are based on a lens type matching section obtained from a dielectric substrate shaping, which results in better matching performances in the entire bandwidth and better mechanical strength than FLuS with a QWT matching section.

The proposed structure is particularly suited in all broadband applications where mechanical strength is an important issue, like space and military applications, since the
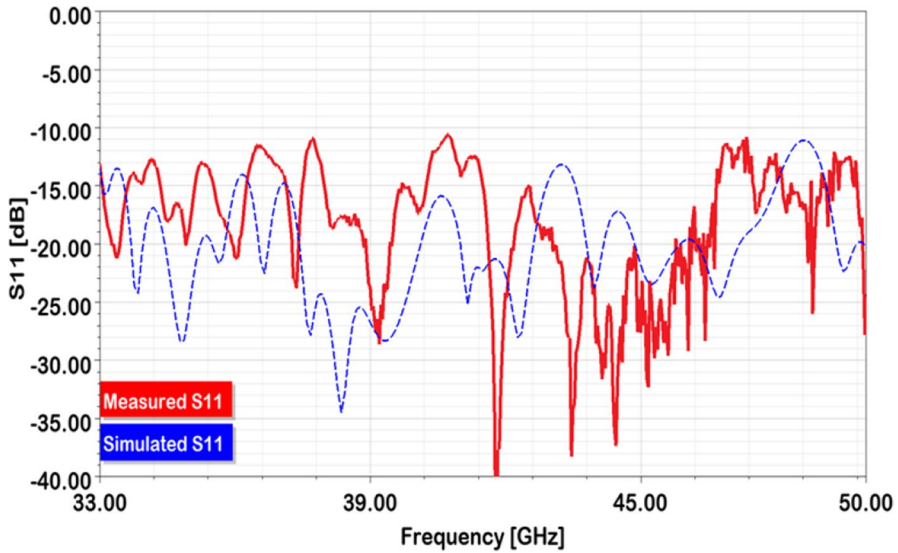
Fig. 25 Return loss of Q band SPC, measured (continuous line) and simulated (dash line)

overall architecture results sturdier to mechanical vibrations. A Q band spatial power combiner was designed and manufactured based on double FLuSes with PDL matching. Excellent results were obtained from this prototype, proving the improvements over the QWT matching foreseen from theoretical investigations and simulation.

To the authors' best knowledge, this is the first time a lens type FLuS has been measured and reported in the literature.
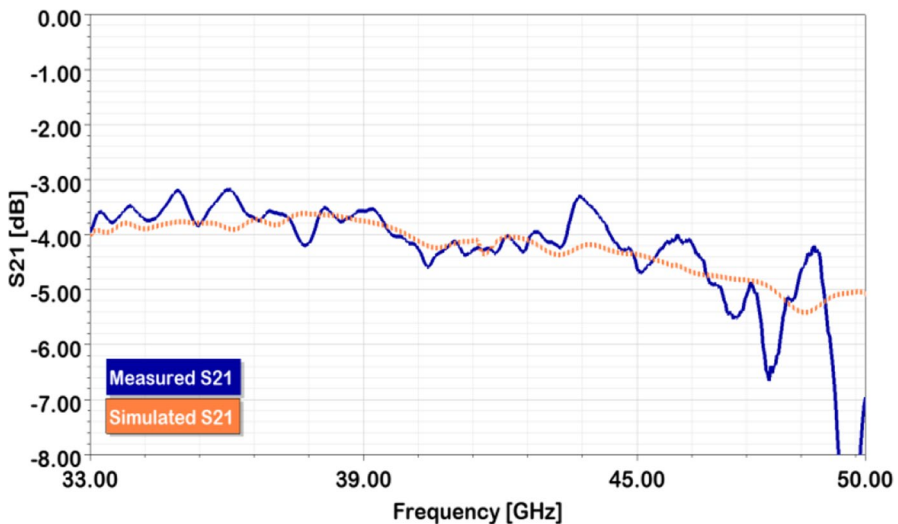

Fig. 26 Insertion loss of Q band SPC, measured (continuous line) and simulated (dash line)

Table 4 Comparison between the state of the art of waveguide-to-microstrip transitions in the Q band and nearest Ka band

Reference	Band (GHz)	Type	Fractional bandwidth
[34]	26–40	E-Probe	0.42
[35]	26–36	E-Probe	0.32
[36]	26–40	Single FLuS	0.42
[37]	40–50	E-Probe	0.22
[38]	30–40	E-Probe	0.28
Proposed	33–47	Dual FLuS	0.35

Data Availability All data generated or analyzed during this study are included in this published article.

Declarations

Ethics Approval The work and the drafting of this paper follow the ethical and professional principles of the authors and other external people involved. The research does not involve human participants.

Consent to Participate No external participation is foreseen for this work.

Consent for Publication If the research is accepted for publication, I consent to publish this work in the *Journal of Infrared, Millimeter, and Terahertz Waves*.

Competing Interests The authors declare no competing interests.

References

1. D. Passi, A. Leggieri, F. Di Paolo, A. Tafuto, and M. Bartocci, "Spatial power combiner technology," in *Progress in Electromagnetics Research Symposium*, 2015, vol. 2015-January.

2. L. Valletti *et al.*, "Vircator Technologies Comparison and Novel Anode Analysis," in *Progress in Electromagnetics Research Symposium*, 2021, vol. 2021-November, https://doi.org/10.1109/PIERS 53385.2021.9694817.

3. F. Marrese *et al.*, "Multiphysics Design of High-Power Microwave Vacuum Window," *J. Microwaves, Optoelectron. Electromagn. Appl.*, vol. 21, no. 1, 2022, https://doi.org/10.1590/2179-10742 022v21i1256395.

4. P. J. Gibson, "The Vivaldi Aerial," in *1979 9th European Microwave Conference*, Sep. 1979, pp. 101–105, https://doi.org/10.1109/EUMA.1979.332681.

5. W. Amara, N. Eltresy, A. Yahyaoui, H. Rmili, T. Aguili, and J. M. Floch, "Design of ultra wideband Vivaldi nanoantenna for solar energy collection," in *IET Conference Publications*, 2017, vol. 2017, no. CP732, https://doi.org/10.1049/cp.2017.0286.

6. R. Citroni, A. Leggieri, D. Passi, F. Di Paolo, and A. Di Carlo, "Nano energy harvesting with plasmonic nano-antennas: A review of MID-IR rectenna and application," *Advanced Electromagnetics*, vol. 6, no. 2. 2017, https://doi.org/10.7716/aem.v6i2.462.

7. R. Citroni, F. Di Paolo, and P. Livreri, "Evaluation of an optical energy harvester for SHM application," *AEU - Int. J. Electron. Commun.*, vol. 111, 2019, https://doi.org/10.1016/j.aeue.2019.152918.

8. R. Citroni, F. Di Paolo, and A. Di Carlo, "Replacing noble metals with alternative metals in MID-IR frequency: A theoretical approach," in *AIP Conference Proceedings*, 2018, vol. 1990, https://doi.org/10.1063/1.5047758.

9. T. Okayama and M. V. Rao, "Power added efficiency and linearity tradeoffs in GaN and GaAs microwave power HEMTs," *Solid. State. Electron.*, vol. 54, no. 3, pp. 294–298, 2010, doi: https://doi.org/10.1016/j.sse.2009.10.006.

10. S. Fantauzzi, L. Valletti, and F. Di Paolo, "Virtual prototype of innovative ka-band power amplifier based on waveguide polarizer," *Adv. Electromagn.*, vol. 9, no. 2, pp. 60–65, 2020, doi: https://doi.org/10.7716/aem.v9i2.1497.

11. D. Passi, A. Leggieri, F. Di Paolo, M. Bartocci, and A. Tafuto, "Design of High Power Density Amplifiers: Application to Ka Band," *J. Infrared, Millimeter, Terahertz Waves*, vol. 38, no. 10, pp. 1252–1263, 2017, doi: https://doi.org/10.1007/s10762-017-0402-1.

12. A. Leggieri, D. Passi, and F. Di Paolo, "The squarax amplifier: An electromagnetic and thermo-mechanical innovation," in *Progress in Electromagnetics Research Symposium*, 2014, pp. 2273–2280.

13. A. Leggieri, D. Passi, G. Saggio, and F. Di Paolo, "Multiphysics design of a spatial combiner predisposed for thermo-mechanically affected operation," *J. Electromagn. Waves Appl.*, vol. 28, no. 17, 2014, https://doi.org/10.1080/09205071.2014.956900.

14. A. Leggieri, D. Passi, G. Saggio, and F. Di Paolo, "Global design of a waveguide X-band power amplifier," *Int. J. Simul. Syst. Sci. Technol.*, vol. 15, no. 4, pp. 68–74, 2014, doi: https://doi.org/10.5013/IJSSST.a.15.04.09.

15. A. Leggieri, G. Orengo, D. Passi, and F. Di Paolo, "The Squarax Spatial Power Combiner," *Prog. Electromagn. Res. C*, vol. 45, pp. 43–55, 2013, doi: https://doi.org/10.2528/PIERC13090 404.

16. D. Passi, A. Leggieri, F. Di Paolo, M. Bartocci, A. Tafuto, and A. Manna, "High efficiency Ka-band spatial combiner," *Adv. Electromagn.*, vol. 3, no. 2, 2014, https://doi.org/10.7716/aem.v3i2.267.

17. A. Leggieri, D. Passi, F. Di Paolo, M. Bartocci, A. Tafuto, and A. Manna, "A novel Ka-band spatial combiner amplifier: Global design and modeling," in *Progress in Electromagnetics Research Symposium*, 2015, vol. 2015-January.

18. C. Yao, J. Xu, and M. Chen, "Design of Ka-band antipodal finline mixer and detector," *J. Semicond.*, vol. 30, no. 5, pp. 28–32, 2009, doi: https://doi.org/10.1088/1674-4926/30/5/055009.

19. B. K. Tan and G. Yassin, "Unilateral finline transition at THz frequencies," *Proc. 20th Int. Symp. Sp. Terahertz Technol.*, no. April, pp. 263–266, 2009.

20. D. Passi, A. Leggieri, R. Citroni, and F. Di Paolo, "Broadband TE10 to TE20 mode transformer for X band," *Adv. Electromagn.*, vol. 5, no. 3, 2016, https://doi.org/10.7716/aem.v5i3.419.

21. S. Xiang, N. F. Shun, and D. Xiu, "A 75–105GHz broad-band balanced mixer in a novel configuration," in *2012 International Conference on Microwave and Millimeter Wave Technology, ICMMT 2012 - Proceedings*, 2012, vol. 5, https://doi.org/10.1109/ICMMT.2012.6230377.

22. D. Passi, A. Leggieri, R. Citroni, and F. Di Paolo, "New six-way waveguide to microstrip transition applied in X band spatial power combiner," *Adv. Electromagn.*, vol. 6, no. 4, 2017, https://doi.org/10.7716/aem.v6i4.421.

23. E. J. Wilkinson, "An N-Way Hybrid Power Divider," *IRE Trans. Microw. Theory Tech.*, vol. 8, no. 1, 1960, https://doi.org/10.1109/TMTT.1960.1124668.

24. B. Bhat and S. K. Koul, *Analysis, Design and Applications of Fin Lines*. Artech House, 1987.

25. F. Di Paolo, *Networks and devices using planar transmission lines*. CRC Press, Taylor-Francis, 2000.

26. S. Fantauzzi, L. Valletti, D. Passi, and F. Di Paolo, "An Innovative Odd-Power Divider by means of a Triple FinLine Waveguide to Microstrip Transition," vol. 11, no. 1, pp. 58–65, 2022, https://doi.org/10.7716/aem.v11i1.1742.

27. C. Lopez, V. Desmaris, D. Meledin, A. Pavolotsky, and V. Belitsky, "Waveguide-to-substrate transition based on unilateral substrateless finline structure: Design, fabrication, and characterization," *IEEE Trans. Terahertz Sci. Technol.*, vol. 10, no. 6, pp. 668–676, 2020, doi: https://doi.org/10.1109/TTHZ.2020.3020683.

28. S. Ramon, J. R. Whinnery, and T. Van Duzer, *Fields and Waves in Communication Electronics*. John Wiley & Sons Inc, 1994.

29. A. Boriskin and R. Sauleau, *Aperture Antennas for Millimeter and Sub-Millimeter Wave Applications*. Springer, 2018.

30. I. O. Adebolu, H. Masui, and M. Cho, "Quantitative evaluation of srs similarity for aerospace testing applications," *Shock Vib.*, vol. 2021, 2021, https://doi.org/10.1155/2021/6655878.

31. A. Leggieri, D. Passi, and F. Di Paolo, "Multiphysics modeling based design of a key-holes magnetron," 2014, https://doi.org/10.1109/NEMO.2014.6995658.

32. A. Leggieri, D. Passi, F. Di Paolo, B. Spataro, and E. Dyunin, "Design of a sub-millimetric electron gun with analysis of thermomechanical effects on beam dynamics," *Vacuum*, vol. 122, 2015, https://doi.org/10.1016/j.vacuum.2015.09.013.

33. S. Fantauzzi, L. Valletti, and F. Di Paolo, "High Power Density Spatial Combiner For The Q-Band, Ready For Space Applications," *Prog. Electromagn. Res. M*, vol. 109, no. February, pp. 163–177, 2022, doi: https://doi.org/10.2528/PIERM21120903.

34. K. Yin, K. Zhang, and J. P. Xu, "Characterization and design of millimeter-wave full-band waveguide-based spatial power divider/combiner," *Prog. Electromagn. Res. C*, vol. 50, no. May, pp. 65–74, 2014, doi: https://doi.org/10.2528/PIERC14031604.

35. X. Jie, C. Yinjie, Q. Cheng, and L. Wenyuan, "A Ka-band power-combined amplifier based on a six-way quasi-planar power divider/Combiner," in *2015 Asia-Pacific Microwave Conference (APMC)*, Dec. 2015, pp. 1–3, https://doi.org/10.1109/APMC.2015.7411821.

36. R. Bai, Y.-L. Dong, and J. Y. Xu, "Broadband Waveguide-to-Microstrip Antipodal Finline Transition without Additional Resonance Preventer," in *2007 International Symposium on Microwave, Antenna, Propagation and EMC Technologies for Wireless Communications*, Aug. 2007, pp. 385–388, https://doi.org/10.1109/MAPE.2007.4393629.

37. J. Xu, Z. Xu, J. Guo, H. C. Zhang, C. Qian, and D. Zhao, "Design of a Q-band six-way spatial power combining structure," in *2018 IEEE MTT-S International Wireless Symposium (IWS)*, May 2018, pp. 1–3, https://doi.org/10.1109/IEEE-IWS.2018.8400955.

38. Z. Kang, Q. Chu, and Q. Wu, "A compact Ka-band broadband waveguide-based traveling-wave spatial power combiner with low loss symmetric coupling structure," *Prog. Electromagn. Res. Lett.*, vol. 36, no. December 2012, pp. 181–190, 2013, https://doi.org/10.2528/PIERL12111311.